Title

Engineering Pseudomonas putida for efficient aromatic conversion to bioproduct using high throughput screening in a bioreactor

Authors

Eng, Thomas
Banerjee, Deepanwita
Lau, Andrew K
et al.

Publication Date

2021-07-01

DOI

10.1016/j.ymben.2021.04.015

Peer reviewed

Metabolic Engineering 66 (2021) 229–238

Contents lists available at ScienceDirect

Metabolic Engineering

journal homepage: www.elsevier.com/locate/meteng

Engineering *Pseudomonas putida* for efficient aromatic conversion to bioproduct using high throughput screening in a bioreactor

Thomas Eng [a,b,1], Deepanwita Banerjee [a,b,1], Andrew K. Lau [a,b], Emily Bowden [a,b], Robin A. Herbert [a,b], Jessica Trinh [a,b], Jan-Philip Prahl [b,c], Adam Deutschbauer [d], Deepti Tanjore [b,c], Aindrila Mukhopadhyay [a,b,d,*]

[a] Joint BioEnergy Institute, Lawrence Berkeley National Laboratory, 5885, Hollis Street, Emeryville, CA, USA
[b] Biological Systems and Engineering Division, Lawrence Berkeley National Laboratory, 1 Cyclotron Rd, Berkeley, CA, USA
[c] Advanced Biofuels and Bioproducts Process Development Unit, Lawrence Berkeley National Laboratory, Hollis Street, Emeryville, CA, 5885, USA
[d] Environmental Genomics and Systems Biology Division, Lawrence Berkeley National Laboratory, 1 Cyclotron Rd, Berkeley, CA, USA

ARTICLE INFO

Keywords:
Para-coumarate
Bioreactor
RB-TnSeq
Pseudomonas putida
Metabolic engineering

ABSTRACT

Pseudomonas putida KT2440 is an emerging biomanufacturing host amenable for use with renewable carbon streams including aromatics such as *para*-coumarate. We used a pooled transposon library disrupting nearly all (4,778) non-essential genes to characterize this microbe under common stirred-tank bioreactor parameters with quantitative fitness assays. Assessing differential fitness values by monitoring changes in mutant strain abundance identified 33 gene mutants with improved fitness across multiple stirred-tank bioreactor formats. Twenty-one deletion strains from this subset were reconstructed, including GacA, a regulator, TtgB, an ABC transporter, and PP_0063, a lipid A acyltransferase. Thirteen deletion strains with roles in varying cellular functions were evaluated for conversion of *para*-coumarate, to a heterologous bioproduct, indigoidine. Several mutants, such as the Δ*gacA* strain improved fitness in a bioreactor by 35 fold and showed an 8-fold improvement in indigoidine production (4.5 g/L, 0.29 g/g, 23% of maximum theoretical yield) from *para*-coumarate as the carbon source.

1. Introduction

Synthetic biology has the potential to produce many new molecules of interest which are challenging to synthesize by traditional chemistry. However, economical bioproduction at industrial scale depends on optimizing many parameters, including growth under bioreactor conditions, achieving high product titers, rates, and yields (TRY), as well as utilization of as many carbon streams derived from renewable carbon feedstocks. While many new molecules can be produced at the laboratory scale, successful development of an economically-viable strain at industrial scale (20,000 L - 2,000,000 L) is estimated to cost as much as 1 billion dollars (Crater and Lievense, 2018).

From an economics perspective, one of the most impactful ways to improve the viability of a process is to reduce the cost of the carbon biomass used as a substrate (Baral et al., 2019b). The use of lignocellulosic biomass in place of pure sugars as a low-cost feedstock could make these microbial processes financially feasible for commodity and bulk chemicals, including biofuels (Baral et al., 2019a). Currently, sugars are extracted from the cellulose and hemicellulose fractions, whereas the lignin fraction has proved to be challenging to convert biologically. Lignin depolymerization can yield structurally distinct aromatic compounds, each of which could be used as a carbon source (Sun et al., 2018). However, a solution from a recent report indicates that base-catalyzed lignin depolymerization could simplify this process, allowing for the recovery of a single dominant aromatic molecule, *para*-coumarate (*p*CA) (Park et al., 2020). In this context, emerging industrial microbes such *P. putida* that can natively utilize such aromatics (Linger et al., 2014) provide an ideal biomanufacturing host platform.

Recently, *P. putida* was engineered to convert aromatic compounds to heterologous metabolites (Johnson et al, 2017, 2019), but process validation for production in larger bioreactor formats is rare. For example, at the 300 L scale, production of a native compound, medium chain length polyhydroxy alkanoates (mcl-PHA) was optimized, but it was under a glucose feed regime (Follonier, 2015). Moreover, there are

* Corresponding author. Joint BioEnergy Institute, Lawrence Berkeley National Laboratory, 5885, Hollis Street, Emeryville, CA, USA.
E-mail address: amukhopadhyay@lbl.gov (A. Mukhopadhyay).
[1] Authors contributed equally.

https://doi.org/10.1016/j.ymben.2021.04.015
Received 13 March 2021; Received in revised form 30 April 2021; Accepted 30 April 2021
Available online 6 May 2021

inherent differences in the conditions used to cultivate a microbial strain in a shake flask vs. the conditions in which bioproduction will finally be deployed (e.g. uniform C source, pH, DO) (Wehrs et al, 2019, 2020). This could be especially impactful on obligate aerobes such as *P. putida* (Nikel and de Lorenzo, 2013). To de-risk the scaling-up of any new microbial process, insights derived from cell physiology in stirred tank bioreactors could clarify how native cellular processes in *P. putida* are different from laboratory cultivation conditions. Here we use the massively parallel RB-TnSeq approach to examine the role of nearly all non-essential gene mutants in fitness across bioreactor cultivation across a range of conditions. The quantitative fitness method using pooled barcoded transposon library we use is called RB-TnSeq and has been described for *P. putida* KT2440 (Price et al. (2019). Querying this pooled *P. putida* mutant library could identify genes beyond metabolism that are required for robust growth in bioreactors.

We extend this fitness profiling data to identify gene mutants implicated in improved bioreactor fitness, and then construct a small library of barcoded deletion strains. We then tested if deletion strains with improved fitness could also be leveraged for improved product formation. Specifically we examined the bioconversion of *p*CA to a heterologous product, indigoidine (Pang et al., 2020; Takahashi et al., 2007; Wehrs et al., 2018), in bioreactors. We describe our high throughput functional genomics screen as well as the strains that led to improved bioreactor and improved product titers using the lignin derived aromatic, *p*CA as a carbon source.

2. Materials and methods

2.1. Chemicals, media and culture conditions

All chemicals were purchased from Sigma-Aldrich (St. Louis, MO) unless mentioned otherwise. When cells were cultivated in a microtiter dish format, plates were sealed with a gas-permeable film (Breathe-easy Sealing membrane, Sigma-Aldrich, St. Louis, MO). Tryptone and yeast extract were purchased from BD Biosciences (Franklin Lakes, NJ). For the analysis of RB-TnSeq mutants, standard M9 minimal medium (1 g/L NH_4Cl, 3 g/L KH_2PO_4, 0.5 g/L NaCl, 12.8 g/L Na_2HPO_4 $7H_20$, 2 mM $MgSO_4$, 0.1 mM $CaCl_2$) with 1% (w/v) glucose was used (Sambrook and Russell, 2001). For the production of indigoidine, engineered strains were grown on modified M9 minimal medium (Linger et al., 2014; Mohamed et al., 2020) with 10 g/L *para*-coumarate shaken at 200 rpm and 30 °C. Modified M9 Minimal Medium contains 2 g/L $(NH_4)_2SO_4$, 6.8 g/L Na_2HPO_4 3 g/L KH_2PO_4, 0.5 g/L NaCl, 2 mM $MgSO_4$, 0.1 mM $CaCl_2$, and 1X trace metals solution (Catalog Num. T1001, Teknova Inc, Hollister CA) with a carbon source as specified. Overnight LB cultures of *P. putida* were grown and adapted in 5 mL modified M9 minimal medium from single colonies. After three sequential rounds of adaptation, cultures were used to inoculate cultures for indigoidine production runs at a starting OD_{600} of 0.1. All experiments were performed in triplicates and in different production scales. The 2 mL cultures grown in 24-well deep well plates (Axygen Scientific, Union City, CA) were incubated with linear shaking at 999 rpm, 70% humidity; 60 mL cultures were grown in unbaffled 250 mL Erlenmeyer shake flasks with orbital shaking at 200 rpm.

2.2. Microbial strains and generation of deletion mutants

Pseudomonas putida KT2440 was used in this study. Genomic deletion mutants were designed to remove DNA sequences corresponding to protein coding regions from the start to the stop codon as previously described (Mohamed et al., 2020). Allelic exchange plasmids were constructed using either backbone pEX18GM or pK18mobsacB and introduced into *P. putida* via conjugation with *E. coli* S17-1 as previously described (Mohamed et al., 2020). Deletion mutants replaced the open reading frame with a DNA barcode, which is a unique 10 bp sequence flanked on either side with ~180bp of DNA sequence derived from the *Saccharomyces cerevisiae SMC1* gene. The flanking sequence is shared among all deletion plasmids simplifying mutant tracking with a universal primer set. Genes that were identified as essential for growth in this study were cross referenced with published gene essentiality data (Molina-Henares et al., 2010). The deletion plasmids and their corresponding barcode sequences, along with the strains described in this study, are contained in Supplementary Table 7 and available post-publication from public-registry.jbei.org.

2.3. Advanced micro bioreactor method: 250 mL ambr® 250 bioreactor cultivations

Fed-batch bioreactor experiments used a 12-way ambr® 250 bioreactor system equipped with 250 mL single-use, disposable bioreactors (microbial vessel type). The vessels were initially filled with 150 mL modified M9 minimal medium containing 8.2 g/L *p*CA as carbon source. Temperature was maintained at 30 °C throughout the fermentation process and agitation was set constant to 1300 rpm. Airflow was set constant to 0.5 VVM based on the initial working volume and pH was maintained at 7.0 using 4 N NaOH. Reactors were inoculated manually with 5 mL of pre-culture cell suspension for an initial OD_{600} of ~0.1. After an initial batch phase of 12 h, cultures were fed with a concentrated feed solution (86 g/L *p*CA, 120 g/L ammonium sulfate, 20 mM arabinose) by administering feed boluses every 2 h restoring *p*CA concentrations to 8.2 g/L (feed parameters: 3.1 min at 50 mL/h). Samples were taken 1–2 times every day (2 mL volume) and stored at −20 °C. The ambr® 250 runtime software and integrated liquid handler was used to execute all process steps.

2.4. RB-TnSeq fitness experiment under different bioreactor conditions

RB-TnSeq fitness assays were carried out as previously reported (Eng et al., 2020; Wetmore et al., 2015). Briefly, pooled *P. putida* KT2440 pooled transposon libraries were thawed from 500 μL glycerol stocks and inoculated into 25 mL LB medium. Cultures were adapted for growth in M9 minimal medium as described in section 2.1. These seed cultures were sampled at 48 h and 72 h (Sample numbers 1 through 6). Each of the bioreactors were inoculated to a starting optical density 600 nm at ~0.2. A 2 L bioreactor equipped with a Sartorius BIOSTAT B® fermentation controller (Sartorius Stedim Biotech GmbH, Goettingen, Germany), fitted with two Rushton impellers fixed at an agitation speed of 800 rpm was used. The temperature was held constant at 30 °C. The bioreactor pH was monitored using the Hamilton EasyFerm Plus PHI VP 225 Pt100 (Hamilton Company, Reno, NV) and was maintained at a pH of 7 using 10 M sodium hydroxide. Dissolved oxygen concentration was monitored using Hamilton VisiFerm DO ECS 225 H0. The initial reactor volume was 1 L M9 minimal medium, with a 50 mL overnight pre-culture in the same medium. The dissolved oxygen (DO) was maintained at either 10% DO (Sample numbers 7 through 11) or 30% DO (Sample numbers 12 through 14) in respective bioreactors. For fed-batch experiments (Sample numbers 15 and 16), the feeding solution contained 100 g/L glucose, and 300 mM ammonium chloride. The feed rate was set at 5.04 g/L/hr of glucose and 3 mM NH_4Cl with a target DO (dissolved oxygen) of 10% or 30% as indicated. Samples for RB-TnSeq analysis were harvested by collecting 1 mL samples, and a cell pellet was collected by centrifugation. Refer to Supplementary Table 1 for a full description of parameters used in each experiment. As needed, a 1 mL bolus of anti-foam B (Sigma Aldrich) was injected into the bioreactor to control excessive foam formation. Several bioreactor runs were excluded from this analysis if the barcode diversity in the RB-TnSeq data pipeline failed quality check steps. Genomic DNA was extracted and processed for library generation and barcode quantification by Illumina sequencing as previously described (Wetmore et al., 2015). The fitness data described in this work will be available upon publication at http://fit.genomics.lbl.gov.

To assess the statistical significance of each fitness value, a *t*-like test

statistic (t score) of the form fitness/sqrt (estimated variance) was used as described previously (Wetmore et al., 2015). A gene mutant was considered to have an enhanced fitness phenotype in an experiment if fitness >1.5, $t > 2$ and have a fitness defect when fitness value was < −2, $t < -2$ (and |fitness| > 95th percentile(|fitness|) + 0.5, as described previously (Price et al., 2018). Hierarchically clustered heatmaps were generated with average linkage method and euclidean distance metric using Python library Seaborn 0.11.1 (Waskom et al., 2020).

2.5. Constraint based modeling to select deletion strains for genes encoding metabolic functions

P. putida KT2440 genome scale metabolic model (GSM) iJN1462 (Nogales et al., 2020) was modified to account for indigoidine biosynthesis. Aerobic growth with either glucose or *para*-coumarate (*p*CA) as the sole carbon source was used to model growth. The ATP maintenance demand was kept the same (0.97 mmol/gDW/h) whereas glucose uptake rate and *p*CA uptake rate were set at 6.3 mmol/gDW/h (del Castillo et al., 2007) and 4.04 mmol/gDW/h (Ravi et al., 2017) respectively. Flux Balance Analysis (FBA) was used to calculate the maximum theoretical yield (MTY) from reaction stoichiometry and redox balance and also for single gene deletion analysis. Minimization of metabolic adjustment (MOMA) analysis (Segrè et al., 2002) was used to predict single gene deletions with minimum perturbation in the metabolic flux distribution compared to wild type. Flux variability analysis (FVA) was used to check for minimum and maximum indigoidine flux for each gene deletion strain. COBRA Toolbox v.3.0 (Heirendt et al., 2019) in MATLAB R2017b was used for FBA, FVA and MOMA

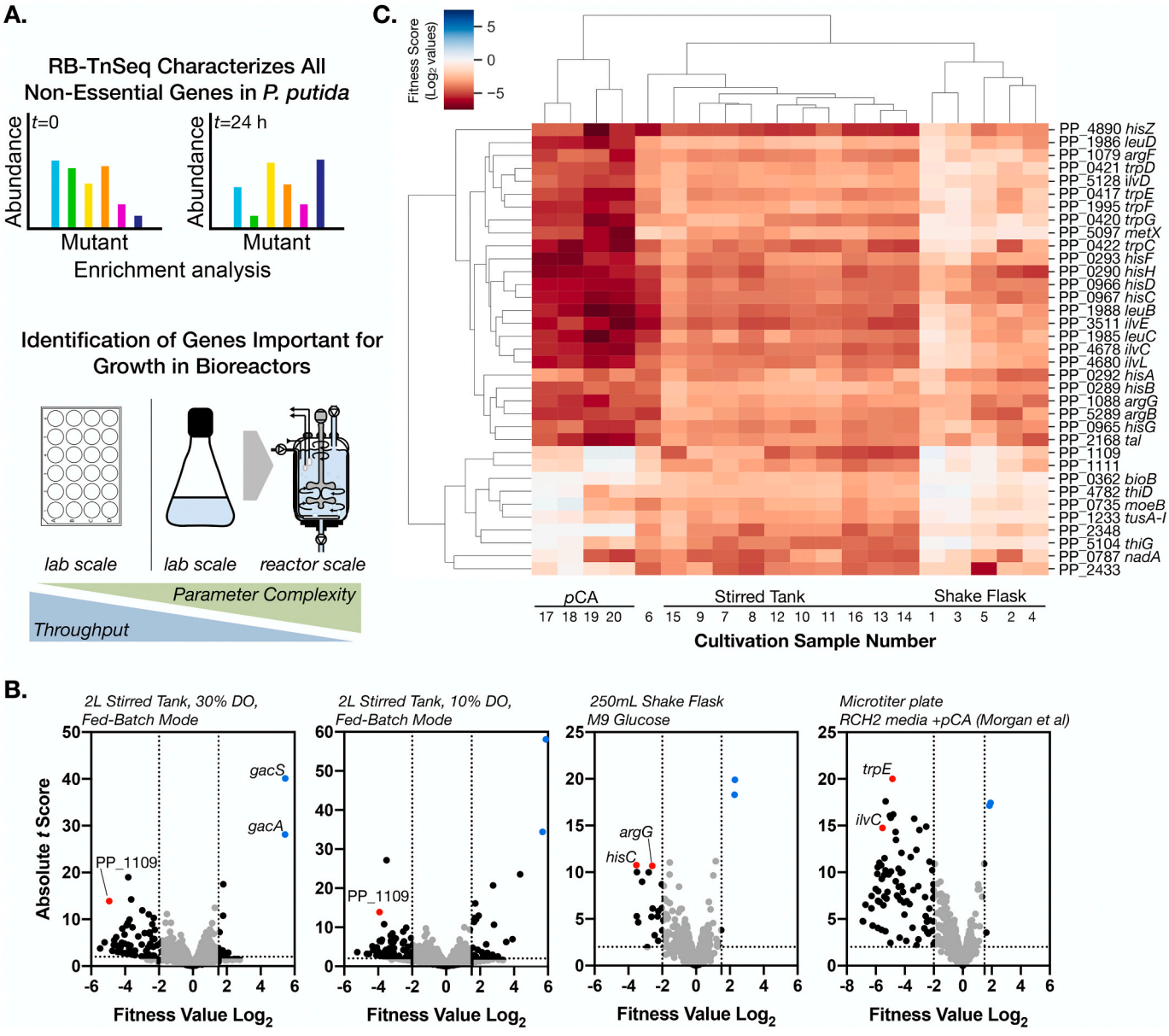

Fig. 1. Comparative *Pseudomonas putida* Mutant Growth Profiling Between Formats Identifies Pathways Needed for Robust Growth. a) RB-TnSeq tracks differential mutant abundance across timepoints and conditions (refer to Table 1) normalized to the initial abundance at T_0. b) Volcano plots of four representative RB-TnSeq experiments. Strong fitness benefits or defects are indicated with dotted lines indicating cutoff $\log_2$ values > 1.5 or < −2.0. For absolute *t* scores, the threshold chosen was $t > 2$. Mutants in a two-component signaling system, GacS-GacA, were found to be associated with fitness benefit (blue) whereas several mutants were found to be associated with fitness defects (red). c) Hierarchically-clustered heatmap generated using average linkage and euclidean distance metric for 35 gene mutants that were fitness-compromised for bioreactor conditions and their corresponding fitness profile under glucose or *p*CA fed laboratory cultivation. (For interpretation of the references to colour in this figure legend, the reader is referred to the Web version of this article.)

simulations with Gurobi (http://www.gurobi.com/) optimization solver.

2.6. Indigoidine quantification

Indigoidine was quantified exactly as described in (Banerjee et al., 2020). In brief, 100 μL of cells were pelleted by centrifugation at 15,000 rpm for 2 min and resuspended in 500 μL DMSO. The solution was vortexed vigorously to dissolve indigoidine. After centrifugation at 15,000 rpm for 2 min, 100 μL of DMSO extracted indigoidine was added to 96-well flat-bottomed microplates (Corning Life Science Products, Corning, NY). Indigoidine was quantitated by measuring the optical density at 612 nm wavelength (OD_{612}) using a microplate reader (Molecular Devices Spectramax M2E) preheated to 25 °C. Accounting for the any dilution applied, indigoidine was quantitated using Eq. (1);

$$Y(g/L \text{ of indigoidine}) = 0.212 * OD_{612} - 0.0035 \quad (1)$$

Indigoidine yields were calculated assuming complete utilization of glucose or *p*CA based on the amount of fed substrate in a minimal medium containing no other carbon sources.

3. Results and discussion

3.1. A core cellular signature for growth under varied process parameters in bioreactors using functional genomics

We designed an experimental regime to identify *P. putida* mutants with changed fitness under conditions relevant to industrial cultivation. In contrast to lab scale experiments biomanufacturing processes for microbes implements cultivation in impeller-mixed jacketed tanks, where gases (ie, ambient air, oxygen) and nutrients (sugars, nitrogen sources) are added to the microbial culture during a given process (González-Cabaleiro et al., 2017; Wehrs et al, 2019, 2020).

Using a pooled barcoded transposon mutant library in *P. putida* KT2440 we were able to rapidly evaluate ~100,000 unique transposon mutants covering nearly all (~4800) non-essential gene mutants with quantitative fitness assays. These cultures of pooled mutants were grown in bioreactors (Fig. 1A) under conditions as outlined in Table 1 to characterize differential fitness changes across timepoints and process conditions. Quantifying changes in barcode abundance allows rapid identification of the specific mutants and their respective fitness values in a workflow referred to as RB-TnSeq (Wetmore et al., 2015). In *P. putida*, this method has been used in predicting carbon catabolic pathways and the characterization of growth inhibitors (Eng et al., 2020; Incha et al., 2020; Thompson et al., 2019). Comparing fitness values from stirred tank conditions to laboratory scale experiments would allow identification of mutants with fitness changes across format and process conditions to distinguish from mutations which generally impacted strain fitness across all conditions.

Table 1
Conditions and cultivation formats for quantitative fitness analysis using the *P. putida* KT2440 RB-TnSeq library.

Sample No.	Culture Format or Scale	Base Media	Sampling Time, Replicate No.[c]	Feed Mode, Carbon Source	Dissolved Oxygen Setpoint
1–6	250 mL shake flask	M9	48 h, 72 h, R1, R2, R3	Batch, Glucose	-
7–11	2 L Sartorius Bioreactor	M9	24 h, 48 h, 72 h, R1, R2	Batch, Glucose	10%
12–14	2 L Sartorius Bioreactor	M9	24 h, R1	Batch, Glucose	30%
15–16	2 L Sartorius Bioreactor	M9	24 h, R1	Fed Batch, Glucose	30%
17–18[a]	24 well plate	RCH2	R1, R2	Batch, *p*CA	-
19–20[b]	96 deep well plate	MOPS	R1, R2	Batch, *p*CA	-

[a] Samples described in Price et al., 2019.
[b] Samples described in Incha et al., 2020. All experiments were conducted at 30 °C.
[c] Replicate numbers are represented as R1, R2 and R3.

For each sample, we calculated the fitness and a corresponding *t* score for single transposon mutants corresponding to all 4778 genes in the pooled library. The calculated fitness value for each timepoint is the $\log_2$ ratio of the population abundance for the sampled timepoint over the initial mutant abundance measured at the start of each experimental time course. The *t* score assesses how reliably a fitness value is different from zero. For most conditions, most gene mutants do not have a measurable differential fitness value and therefore have fitness values and *t* scores close to 0. For our genome-wide analysis, we selected strong, statistically significant determinants of fitness and demanded that fitness values must be > 1.5 or < -2 with an absolute *t* score of >2. Volcano plots of mutant fitness values and their corresponding *t* scores are plotted for five representative experiments in Fig. 1B.

Our high throughput screening approach identified both mutants with improvements (*Section 3.2*) and defects in bioreactor fitness. While we are interested in the former, an analysis of mutants with decreased fitness is important to understand conditional essentiality for a full characterization. From this dataset we identified thirty-five transposon mutants in *P. putida* which displayed growth defects under these conditions (Fig. 1C). Hierarchical clustering of mutants that had decreased fitness (<-2) indicated that most bioreactor samples fed glucose were similar to samples fed glucose in the shake flask format, but had different responses when cells were fed *p*CA. For conditions listed in Table 1, mutants with decreased fitness belonged to genes involved in methionine, tryptophan and histidine biosynthetic pathways. Other multi-step amino acid biosynthesis pathways (leucine, arginine, and aspartate) were also identified with decreased fitness, but for only 1–2 mutants in these pathways. Pathways predicted for sulfur relay and thiamine biosynthesis (PP_0261, PP_1233, PP_5104) or metal ion homeostasis (PP_3506, PP_0910) were also implicated as necessary for robust growth under bioreactor conditions. We note that these single gene inactivations do not result in amino acid or nutrient auxotrophies, as these mutants are still able to grow in M9 minimal media. When these mutants were clustered, mutants in two additional uncharacterized genes (PP_1109, PP_1111) were also present in this group, suggesting they have related functions. Nineteen mutants were unique to growth on *p*CA. These included genes encoding transcriptional regulators or metabolic functions in pathways related to aromatic compound catabolism already described elsewhere (Incha et al., 2020). Including *p*CA fitness profiling data from the Price et al., 2019 dataset also strengthened evidence for statistically significant fitness defects in other genes encoding metabolic functions including PP_5095/*proI* (involved in proline biosynthesis), PP_0356/*glcB* (malate synthase), PP_4700/*panC* (pantothenate synthase) and PP_4799 (a putative muramoyltetrapeptide carboxypeptidase).

Several regulatory systems were also implicated in a novel bioreactor stress response. Deletion of either the σ38 stress response sigma factor (PP_1623/*rpoS*) or a housekeeping sigma factor σ70-family gene (PP_4208) strongly decreased fitness in the bioreactor. In contrast to *E. coli* which has a single known sigma 70 response factor, there are 19 open reading frames which encode σ70 family protein domains, suggesting functional redundancy via duplication (Martínez-Bueno et al., 2002). Other *P. putida* RB-TnSeq datasets did not show the deletion of either sigma factor to have fitness defects (RB-TnSeq fitness browser, https://bit.ly/3bifz2h), suggesting that the fitness enhancement in a bioreactor is enhanced by both σ38 and σ70-family transcriptional regulation, and that their regulatory network is not redundant. Additionally, four environmental/nutrient availability sensing two-component signaling systems also contribute to bioreactor fitness: a nitrogen stress sensor (PP_2388-PP_2390) (Mozejko-Ciesielska et al.,

2018); a sensor involved in chloramphenicol resistance (PP_0185) (Fernández et al., 2012); a sensor implicated in lipid A remodeling (PP_2348); and a two component system important for adaptation to growth in minimal medium (PP_4505-PP_2714). The specific stirred tank parameters which activate these remaining two component signaling systems have not been identified.

Other mutants which decrease fitness in bioreactors included mutations in PP_5303/*ridA*, a reactive oxygen species responsive chaperone, or PP_0735/*moeB*, an adenyltransferase which adenylates molybdopterin synthase, were deficient for growth. Finally, mutations in four other genes could not be assigned a function due to low homology to previously characterized genes or correlation with known processes. Due to the pooled nature of our high-throughput assay, disrupted gene pathways that utilize metabolites which can be complemented by secreted metabolites from other mutants in the population will not be detected in this assay. Moreover, transposon insertions which disrupt poly-cistronic mRNAs can sometimes result in polar effects, a drawback of this high-throughput method (Hutchison et al., 2019). Regardless, our negative fitness mutants identified important genes to avoid inactivating when considering genome scale approaches (Maia et al., 2016) for host optimization.

3.2. Gene mutants with improvements in bioreactor fitness

Microbes are not evolved for environments like the stirred tank bioreactor; a mismatch between endogenous cellular activities and the cultivation environment can lead to inefficiencies in growth. We reasoned that mutants with improved fitness values from the RB-TnSeq dataset are more suited for industrial cultivation parameters. Hierarchical clustering of positive fitness mutants across all bioreactors in comparison with *p*CA and shake flask conditions indicated that a fitness signature in the bioreactor was distinct from either standard laboratory format using the aromatic carbon source or glucose (Fig. 2A). We identified transposon mutants in eighteen genes which consistently exhibited quantitatively improved fitness under these growth conditions in a bioreactor (Fig. 2A). Additionally, mutants in a two component signaling system, *gacS-gacA* (PP_1650-PP_4099), were routinely recovered as a fitness enhanced phenotype under many conditions (Fig. 2A and B).

The data generated from these high throughput assays are crucial to this analysis, as they quantify the contribution from both metabolic and regulatory processes and their relationship to cell growth. Approximately half of the mutants identified from these fitness profiling experiments were related to metabolic processes (Fig. 2C). The remaining non-metabolic candidates encoded a diverse range of cellular functions, such as PP_1215/*ruvC* (a crossover junction endodeoxyribonuclease), PP_1353 (an uncharacterized conserved membrane protein), and PP_5309 (a LysR-family transcriptional regulator). Inactivating PP_1428/*rpoE* (Sigma factor sigma-E) led to a slight fitness improvement in most of the bioreactor conditions tested by RB-TnSeq, but not in the control shake flask experiments. Many of these genes likely encode global master regulators and their deletion have pleiotropic impacts across cell physiology. Interestingly, we did not observe *crc* mutants associated with improvements in our analysis, which is another global regulator previously reported for improvement in production (Elmore et al., 2020; Johnson et al., 2017). We identified potential gene targets summarized in Table 2, whose inactivation would result in improved fitness in a bioreactor including genes encoding metabolic activities as well as genes encoding non-metabolic global regulators across varied oxygen and mixing conditions in bioreactors using RB-TnSeq.

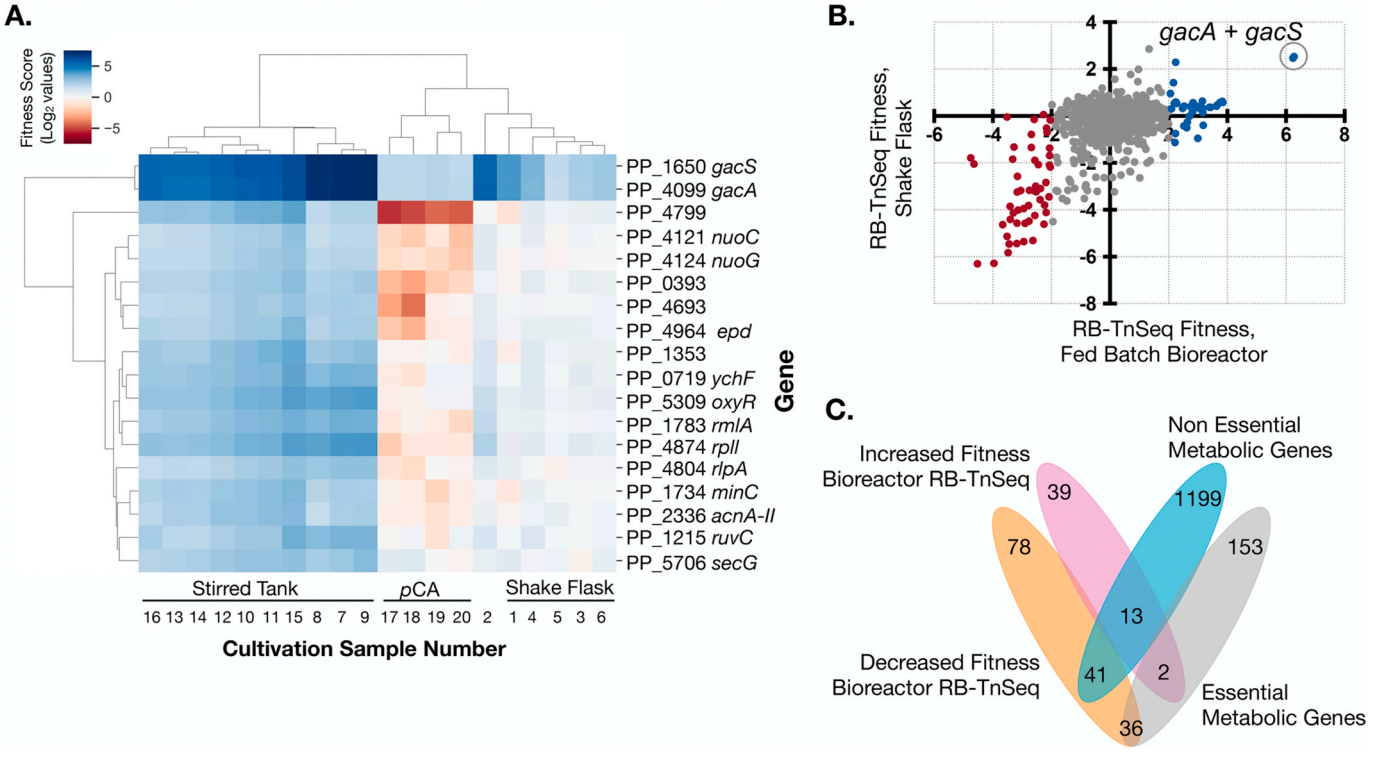

Fig. 2. Identification of *P. putida* Enhanced Growth Mutants. a) Hierarchically-clustered heatmap generated using average linkage and euclidean distance metric for 18 gene mutants with enhanced fitness (fitness value greater than 1.5) across all bioreactor conditions compared to fitness values under laboratory conditions using *p*CA in microtiter plates or glucose in shake flask as the sole carbon source. Refer to Table 1 for a full description of conditions corresponding to the sample numbers. b) Scatter plot showing the fitness values of mutants with enhanced fitness (red, fitness values > 2) or compromised fitness (blue, fitness values < 2) under grown in shake flask *vs.* a fed-batch bioreactor. c) Venn diagram indicating distribution of genes binned into four different categories from the transposon mutant pool using fitness profiling values from bioreactor fitness experiments and gene essentiality. (For interpretation of the references to colour in this figure legend, the reader is referred to the Web version of this article.)

Table 2
Fitness-enhanced deletion mutants in bioreactors.

Gene Locus/Gene Name	Max Fitness Value[a]	Fold Fitness Benefit[b]	Gene Function	Predicted Biomass Yields	
				[g/mmol of glucose]	[g/mmol of *p*CA]
PP_1109	−5.2	16.2	GntR-family transcriptional regulator	NM	NM
PP_2889/*prtR*	4	5.6	Transmembrane regulator; anti-sigma factor	NM	NM
PP_4099/*gacA*	7.2	1.37	Two component signaling system	NM	NM
PP_0063	2.4	1.7	Lipid A biosynthesis lauroyl acyltransferase	0.1	0.11
PP_1385/*ttg1B*	0.9	3.6	RND membrane pump; implicated in *p*CA tolerance	0.1	0.11
PP_1656/*relA*	4.5	0.5	ATP:GTP 3′-pyro phosphotransferase; pppGpp synthetase	0.1[c]	0.11
PP_2336	3.1	8.3	Aconitate hydratase 1	0.1	0.11
PP_4120/*nuoB*	2.7	4	NADH-quinone oxidoreductase subunit B	0.04[c]	0.05
PP_4121/*nuoCD*	2.8	11.6	NADH-quinone oxidoreductase subunit C + D	0.04[c]	0.05
PP_4124/*nuoG*	2.8	13.9	NADH-quinone oxidoreductase subunit G	0.04[c]	0.05
PP_4129	3.2	6.9	NADH-quinone oxidoreductase subunit L	0.04[c]	0.05
PP_5227	1.7	6	Diaminopimelate decarboxylase	0.1	0.11
PP_5338/*aspA*	2.5	4.3	Aspartate ammonia lyase	0.1	0.11

Genes are first sorted based on metabolic or non-metabolic function followed by genomic locus ID. If known, common gene names are also indicated. Refer Supplementary Table 2 for complete list of loci targeted for deletion including newly identified essential genes.
[a] Maximum $\log_2$ fitness value across all bioreactor conditions tested.
[b] Log_2 fitness value in bioreactor versus fitness value in shake flask.
[c] No solution for indigoidine flux using MOMA analysis. NM - Genes associated with non-metabolic function.

3.3. The bioconversion of a lignin derived aromatic to a heterologous bioproduct

The overarching aim of this study is to combine robust bioreactor strains for the conversion of lignin derived aromatics to valuable heterologous bioproducts. Indigoidine, a sustainable pigment and emerging fabric dye, is generated from the condensation of two glutamine molecules and is catalyzed by a heterologous non-ribosomal peptide synthetase (NRPS) based pathway (Ghiffary et al., 2021; Pang et al., 2020; Takahashi et al., 2007; Wehrs et al., 2018) (Supplementary Figure 1). Although we have demonstrated *P. putida* based indigoidine production using glucose as the carbon source (Banerjee et al., 2020), it is useful to have a collection of strains with improved fitness in bioreactors ready for bioprocess engineering. We initially identified fifty-four *P. putida* mutants which simply had increased fitness across many stirred tank process conditions (Fig. 2C). In addition, we included mutants in metabolic processes with higher fitness values in stirred tank bioreactors when compared to the shake flask format. This differential fitness value was calculated as the ratio of $\log_2$ fitness values in a bioreactor over shake flask cultivation as the denominator, which indicated a small number of genes should be included even though they did not have strong absolute fitness improvements or *t* scores that would meet the threshold for inclusion. From this analysis we identified 14 additional genes related to cell metabolism.

We evaluated how deleting these individual genes for their potential impact on maximum biomass yields using the minimization of metabolic adjustment (MOMA) method (Segrè et al., 2002) when fed glucose or *p*CA as carbon sources. MOMA analysis predicted the immediate effect of a gene deletion with minimal perturbation in the metabolic flux distribution compared to wild-type *P. putida* (Supplementary Table 4). Of the 14 genes encoding metabolic functions we examined, only PP_0290 was predicted to be essential *in silico* for growth using both glucose or *p*CA as sole carbon source, which was then excluded from further study.

A strain with improved fitness in a bioreactor does not necessarily translate to improved final product TRY and furthermore, we are not aware of any studies that directly link these phenotypes. We reasoned that additional computational analysis for improvements towards the specific bioproduct of interest could further refine our library. Using a genome scale metabolic model of *P. putida*, iJN1462 (Nogales et al., 2020) and Flux Balance Analysis (FBA), we calculated maximum theoretical yields (MTY) of indigoidine and its precursors for *p*CA as substrate/bioproduct pair (Supplementary Table 3). This carbon source to final product MTY pair (*p*CA/indigoidine) of 0.66 mol/mol is higher than MTY calculated for the glucose/indigoidine pair of 0.54 mol/mol (Banerjee et al., 2020). The predicted flux towards indigoidine in the 15 deletion strains associated with metabolic functions successfully generated is summarized in Supplementary Table 4. For several mutants, indigoidine yields were unlikely to substantially improve yield, but would still allow yields approximately 80–100% of WT. Five of the deletion mutants analyzed (Fig. 2C) had no solution when calculating indigoidine flux using MOMA analysis when fed glucose, but solutions did exist for *p*CA feed conditions. These model predictions suggested there might be improvements to final product titer in these deletion strains.

In total, this study identified an ensemble of 33 genes in our fitness-advantaged barcoded library (Supplementary Table 2). Our mutants have a diverse range of biological functions, fitness values in bioreactors, and biomass predictions from MOMA analysis (Table 2). We reconstructed barcoded deletion mutants for candidate genes using allelic exchange plasmids (Fig. 3A and Supplementary Table 7) and were successful in completing a library of twenty-one deletion mutant strains. To profile heterologous bioproduct formation, as modeled with the 2 gene non-ribosomal peptide (NRP), indigoidine, we screened a majority of the deletion library for improvements to indigoidine titer. The indigoidine pathway was genomically integrated into each deletion strain. As controls, we included Δ*ttgB* to test if reducing *p*CA efflux could allow greater substrate availability for catabolism; ΔPP_1109 which exhibited negative fitness values in the bioreactor; and ΔPP_2889 which in the RB-TnSeq data, was more fit only under batch-mode conditions but not fed-batch modes.

Strains were assayed first in 24-deepwell plates to compare indigoidine production using either glucose or *p*CA as the carbon source. In this format, the WT strain produced about 1.5 g/L of indigoidine from either glucose or *p*CA as the carbon source after 48 h of cultivation. In contrast, Δ*gacA* strains produced 2.5 g/L of indigoidine after 48 h using *p*CA (Fig. 3B) but only 0.5 g/L indigoidine from glucose (Fig. 3C). Deletions of genes encoding several subunits of the NADH-quinone oxidoreductase complex (PP_4120, PP_4124, PP_4129) led to statistically significant but modest improvements in indigoidine titer when cells were fed glucose, but not *p*CA. Deletion strains ΔPP_5338, ΔPP_0063, ΔPP_5227, ΔPP_1656, ΔPP_2336, and ΔPP_1385 also showed some improved indigoidine titer on *p*CA but not on glucose (Fig. 3). Deletion mutants ΔPP_1109 and ΔPP_2889 did not improve indigoidine titer from either carbon source in the deep well plate format

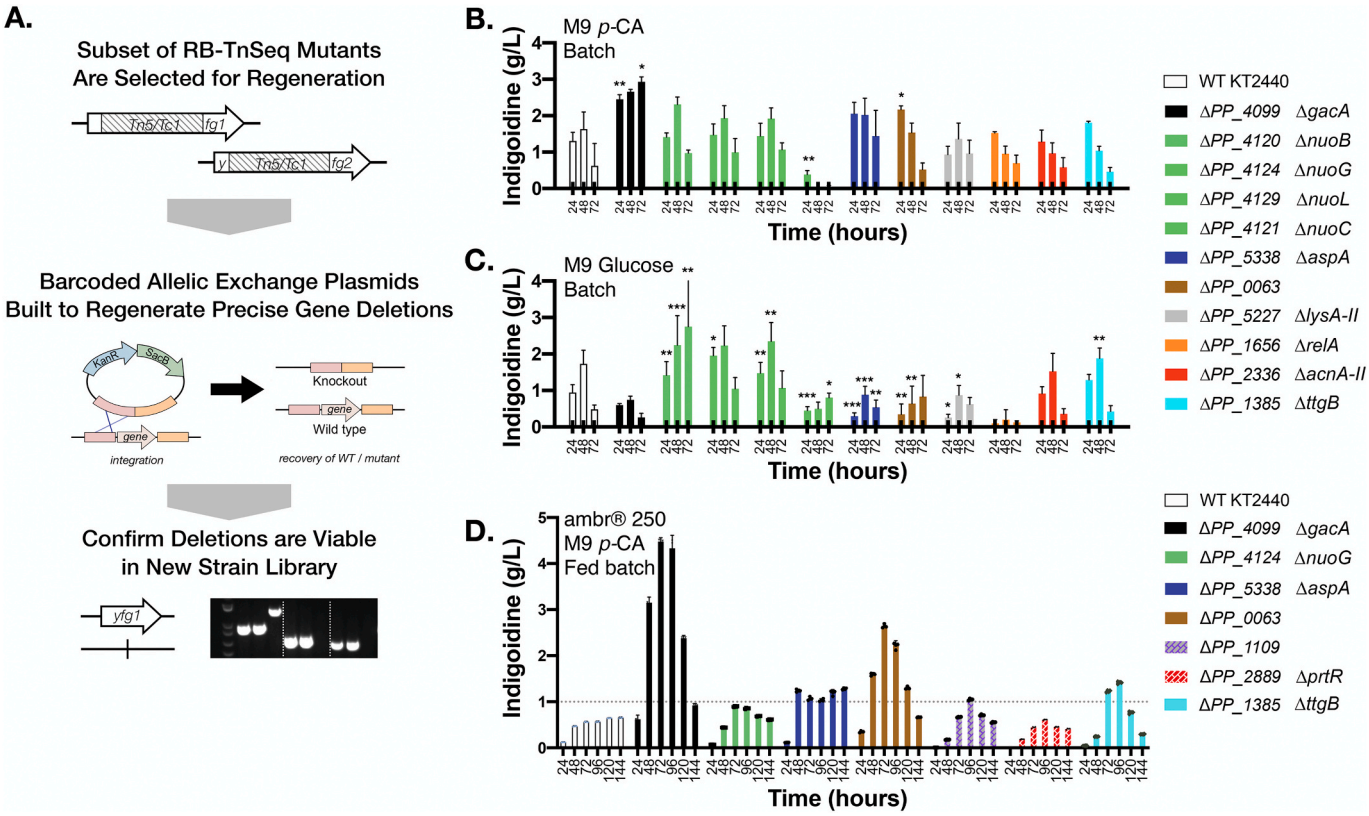

Fig. 3. Assessment of Indigoidine Production in Barcoded Deletion Strains Across Scales. A. Workflow to reconstruct barcoded deletion mutants identified in the RB-TnSeq high throughput assay. B. Indigoidine production in batch mode using *p*CA as carbon source C. Indigoidine production in batch mode using glucose as the carbon source. Single gene deletions in the Nuo holocomplex (PP_4120 - PP_4129) are indicated in green. Otherwise, deletions are arranged by decreasing titer. For B and C, error bars indicate SD and n = 3 from independent biological replicates. Statistically significant improvement in indigoidine titers in comparison to titers in WT *P. putida* KT2440 are represented using P values (* = 0.0123, ** <0.0089 and *** <0.0008). D. Fed-batch mode production of indigoidine using *p*CA as the carbon source from n = 3 technical replicates. For D, all indigoidine titers were statistically significant (P value < 0.0094) in comparison to titers in WT *P. putida* KT2440 at the respective time points except for time point 144 h for ΔPP_4124 and ΔPP_0063. (For interpretation of the references to colour in this figure legend, the reader is referred to the Web version of this article.)

(Supplementary Figure 2). These experiments identified several mutants with improved indigoidine production from *p*CA, which allowed us to further down-select candidate strains for bioreactor runs.

Automation-assisted fed-batch bioreactors (Ambr® 250) enable medium throughput analysis in stirred tank bioreactors and were used to examine the most promising four deletion mutant strains for indigoidine production (Δ*gacA*, ΔPP_4124, ΔPP_5338, and ΔPP_0063). In this scale-up, Δ*gacA* strains produced 4.5 g/L indigoidine after 72 h, whereas the WT strain produced 0.5 g/L in the same timeframe. ΔPP_0063 also showed some improvement over the WT strain with a titer of 2.5 g/L. Deletion strains ΔPP_4124 or ΔPP_5338 did not further improve indigoidine titer in the bioreactor. The remaining control strains performed as expected; a representative deletion strain with a negative fitness value (ΔPP_1109) did not produce more indigoidine than wild type; reducing *p*CA efflux (Δ*ttgB*) or optimizing for growth under batch mode conditions (ΔPP_2889) also failed to improve titer. The indigoidine yield from the control strain was 0.034 g indigoidine/g *p*CA, and the yield from the Δ*gacA* production strain was 0.29 g indigoidine/g *p*CA, an 8.5 fold improvement over wild type. The Δ*gacA* strain reached 29% MTY (g indigoidine/g *p*CA) under fed-batch conditions. This result demonstrates a successful application of fitness profiling of deletion libraries for improved bioconversion route to produce indigoidine when fed a lignin-derived monomer as the sole carbon source. Further, mechanistic studies will reveal the interplay between the specific metabolic processes implicated with these their respective deletion mutants and their relationship to indigoidine titers.

3.4. The role of GacS-GacA in the bioconversion of pCA to indigoidine

Disruption of *gacA* led to the most substantial improvement in fitness and was also a ubiquitous target across the conditions tested. Most importantly, the *gacA* deletion strain improved heterologous product formation from *p*CA. Previous work in *Pseudomonas* spp. has shown that the GacS-GacA two component signaling system is involved in a wide range of environmental responses such as biofilm formation or secondary metabolite secretion (Burlinson et al., 2013; Francis et al., 2017; Gellatly et al., 2018; Huang et al., 2019). A bioinformatics analysis for these potential GacS-GacA downstream targets in *P. putida* based on Huang et al. is summarized in Supplementary Table 6. In *P. putida,* GacS inactivation was shown to enhance the glucose to muconate bioconversion (Bentley et al., 2020). We were intrigued why this highly conserved signaling system was not reported as beneficial towards bioproduct formation in *E. coli*. To answer this query, we conducted a meta-analysis of functional genomics data from all public RB-TnSeq carbon source datasets (https://bit.ly/38oy971 and Supplementary Table 5). In *E. coli*, inactivation of either *gacS* or *gacA* homologs does not lead to any detectable biologically relevant phenotypes (Fig. 4). In contrast, inactivation of either *gacS* or *gacA* in *P. putida* or *P. stutzeri* reveals strong fitness improvements across nearly all experimental conditions. However, a STRINGdb meta-analysis (Szklarczyk et al., 2019) also identified potentially conserved protein-protein interactions between GacA and other relevant candidate effector proteins (Supplementary Figure 3). This signaling system may be tuned to environmental cues specific to *Pseudomonas'* native soil environment and absent from

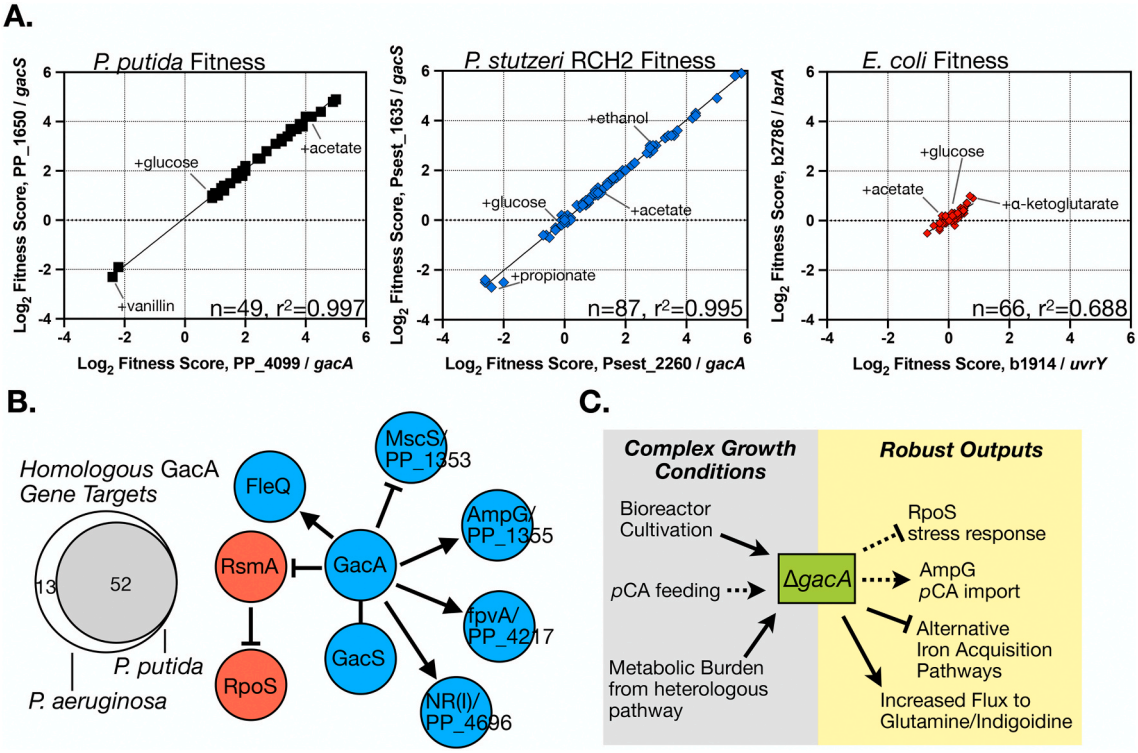

Fig. 4. Functional Differences Between *Pseudomonas* GacS-GacA Signaling Systems And *E. coli* Homolog BarA-UvrY. A. Meta-analysis of cofitness values for GacS-GacA mutants from publicly available RB-TnSeq carbon source datasets. Data from *P. putida*, *P. stutzeri* and *E. coli* are plotted on the same scale. B. Upregulated (blue) and downregulated (red) gene targets of the response regulator GacA based on the meta-analysis. C. Model. Δ*gacA* cells parse many nutrient and environmental signals and improve formation of a glutamine-derived product, indigoidine. (For interpretation of the references to colour in this figure legend, the reader is referred to the Web version of this article.)

the intestinal gut where *E. coli* was isolated. A better understanding of microbial regulatory systems can identify potential bioproduct formation bottlenecks in industrial process conditions. For example, the *P. putida* GacS-GacA system may have little crosstalk with other signaling systems, as mutants in *gacS* and *gacA* have high cofitness as shown in Fig. 4A but other regulatory systems may interact with a wide array of seemingly independent master regulators (r^2 for *P. putida* = 0.997; r^2 for *P. stutzeri* = 0.995; r^2 for *E. coli* = 0.688).

Based on prior reports of GacS-GacA activity in *Pseudomonas,* we hypothesize that an active GacS-GacA signalling system may induce formation of diverse secondary metabolites, biofilm formation and alternative iron sequestration pathways; these pleiotropic processes could limit the carbon flux available for indigoidine production (Fig. 4B). In parallel, the constitutive de-repression of a permease (PP_1355), also regulated by this signaling system (Huang et al., 2019 and Supplementary Table 6), could improve *para*-coumarate utilization. This hypothesis is consistent with RB-TnSeq fitness data, as the inactivation of PP_1355 caused a fitness defect when cells were grown on *p*CA as a carbon source (Price et al., 2019). The *E. coli* PP_1355 homolog, *ampG*, participates in both cell wall turnover and biofilm formation (Mallik et al., 2018), suggesting a complex physiological response could occur in *P. putida*.

It is puzzling that the improvement to indigoidine titer in Δ*gacA* and ΔPP_0063 occurred when fed *p*CA rather than glucose. While additional experiments are required to fully understand this outcome, aromatic molecules like toluene are known to induce a starvation response (Vercellone-Smith and Herson, 1997) and could occur in *p*CA. Without *gacS* present, the *rpoS* response is dampened (Whistler et al., 1998). This model is supported by our experimental data, as inactivation of *gacS* improves *P. putida* fitness when cells are grown on *p*CA (Fig. 2). PP_0063, one of the two secondary lipid A acyltransferases in *P. putida*, has been reported to play a role in the *P. putida* global stress response when cells were fed benzoate, a structurally similar aromatic compound with a different catabolic pathway (Ravi et al., 2017; Reva et al., 2006). It is possible that the increased membrane permeability in the ΔPP_0063 strain improved cell respiration using *p*CA (Budin et al., 2018; Zhu et al., 2017). However, the ΔPP_0063 strain had improved indigoidine titers compared to wild type but lesser than Δ*gacA* strain, suggesting that inactivating PP_0063 is not as beneficial towards indigoidine production as a Δ*gacA* deletion. Methods in quantifying lipid composition (Rühl et al., 2012) may help shed light in understanding the interplay between membrane dynamics, respiration, and the physiological requirements for growth in bioreactors. We synthesize this information in a model depicted in Fig. 4C. In summary, our data suggests that final indigoidine titer improved in the Δ*gacA* strain because a subset of starvation response genes are induced by *p*CA without activating the full complement of GacS-GacA regulatory targets.

4. Conclusions

Our study describes the distinct fitness landscape at the whole-genome level under scaleup conditions, identifying non-obvious connections between many cellular processes, both metabolic and regulatory, to growth in larger format processes. We describe a workflow to down-select mutant strains for examination in medium-throughput stirred tank formats like the ambr250® bioreactor system, and also provide a bioreactor ready strain for the conversion of a lignin-derived aromatic into a valuable sustainable pigment, indigoidine, at high titers, rates and yield. Due to the relative accessibility of sequencing technologies, even larger mutant search spaces could be examined. Examples include the use of double or triple mutant RB-TnSeq libraries, or gene overexpression pools with native or heterologous gene libraries (Dunlop et al., 2011; Isalan et al., 2008; Mutalik et al., 2019) drawing novel gene candidates identified from pan-genome assemblies

(Norsigian et al., 2020). These systems biology approaches hold the promise to considerably advance *P. putida* to meet the bioprocess parameters of tomorrow's bioeconomy.

Data availability

The fitness datasets related to this article can be found at http://fit.genomics.lbl.gov upon publication. List of plasmids and strains used in this study are described in the Supplementary Materials and their sequences can be found at public-registry.jbei.org (registration for a free account is required). Additional requests for datasets and strains generated and analyzed during the current study are available from the corresponding author upon request.

CRediT authorship contribution statement

Thomas Eng: Conceptualization, Data curation, Formal analysis, Investigation, Methodology, Supervision, Validation, Visualization, Writing – original draft, Writing – review & editing. **Deepanwita Banerjee:** Conceptualization, Data curation, Formal analysis, Investigation, Resources, Software, Validation, Visualization, Writing – original draft, Writing – review & editing. **Andrew K. Lau:** Data curation, Formal analysis, Investigation, Methodology, Validation, Visualization, Writing – review & editing. **Emily Bowden:** Investigation, Methodology, Validation. **Robin A. Herbert:** Data curation, Formal analysis, Investigation, Methodology, Resources, Validation. **Jessica Trinh:** Investigation, Methodology, Validation. **Jan-Philip Prahl:** Data curation, Formal analysis, Investigation, Methodology, Validation, Writing – review & editing. **Adam Deutschbauer:** Investigation, Methodology, Resources, Writing – review & editing. **Deepti Tanjore:** Formal analysis, Funding acquisition, Methodology, Supervision, Validation, Writing – review & editing. **Aindrila Mukhopadhyay:** Conceptualization, Data curation, Formal analysis, Funding acquisition, Investigation, Methodology, Project administration, Resources, Supervision, Writing – original draft, Writing – review & editing.

Declaration of competing interest

The authors declare that they have no known competing financial interests or personal relationships that could have appeared to influence the work reported in this paper.

Acknowledgements:

We thank Christopher J. Petzold, Ashish Misra, Megan Garber, Alex Codik, and members of the Mukhopadhyay group for feedback and technical assistance. We thank Jim Colton (Graphpad Software, San Diego, CA) for help with Prism Graphpad for data visualization.

Appendix A. Supplementary data

Supplementary data to this article can be found online at https://doi.org/10.1016/j.ymben.2021.04.015.

Funding

This work was conducted by the Joint Bioenergy Institute and the Joint Genome Institute, supported by the US Department of Energy, Office of Science, through contract DE-AC02-05CH11231 between Lawrence Berkeley National Laboratory and the US Department of Energy. The Advanced Biofuels and Bioproducts Process Development Unit is partially funded by the US Department of Energy, BioEnergy Technology Office.

References

Banerjee, D., Eng, T., Lau, A.K., Sasaki, Y., Wang, B., Chen, Y., Prahl, J.-P., Singan, V.R., Herbert, R.A., Liu, Y., Tanjore, D., Petzold, C.J., Keasling, J.D., Mukhopadhyay, A., 2020. Genome-scale metabolic rewiring improves titers rates and yields of the non-native product indigoidine at scale. Nat. Commun. 11, 5385. https://doi.org/10.1038/s41467-020-19171-4.

Baral, N.R., Kavvada, O., Mendez-Perez, D., Mukhopadhyay, A., Lee, T.S., Simmons, B.A., Scown, C.D., 2019a. Techno-economic analysis and life-cycle greenhouse gas mitigation cost of five routes to bio-jet fuel blendstocks. Energy Environ. Sci. 12, 807–824. https://doi.org/10.1039/C8EE03266A.

Baral, N.R., Sundstrom, E.R., Das, L., Gladden, J.M., Eudes, A., Mortimer, J., Singer, S.W., Mukhopadhyay, A., Scown, C.D., 2019b. Approaches for more efficient biological conversion of lignocellulosic feedstocks to biofuels and bioproducts. ACS Sustain. Chem. Eng. 7, 9062–9079. https://doi.org/10.1021/acssuschemeng.9b01229.

Bentley, G.J., Narayanan, N., Jha, R.K., Salvachúa, D., Elmore, J.R., Peabody, G.L., Black, B.A., Ramirez, K., De Capite, A., Michener, W.E., Werner, A.Z., Klingeman, D. M., Schindel, H.S., Nelson, R., Foust, L., Guss, A.M., Dale, T., Johnson, C.W., Beckham, G.T., 2020. Engineering glucose metabolism for enhanced muconic acid production in Pseudomonas putida KT2440. Metab. Eng. 59, 64–75. https://doi.org/10.1016/j.ymben.2020.01.001.

Budin, I., de Rond, T., Chen, Y., Chan, L.J.G., Petzold, C.J., Keasling, J.D., 2018. Viscous control of cellular respiration by membrane lipid composition. Science 362, 1186–1189. https://doi.org/10.1126/science.aat7925.

Burlinson, P., Studholme, D., Cambray-Young, J., Heavens, D., Rathjen, J., Hodgkin, J., Preston, G.M., 2013. Pseudomonas fluorescens NZI7 repels grazing by C. elegans, a natural predator. ISME J. 7, 1126–1138. https://doi.org/10.1038/ismej.2013.9.

Crater, J.S., Lievense, J.C., 2018. Scale-up of industrial microbial processes. FEMS Microbiol. Lett. 365 https://doi.org/10.1093/femsle/fny138.

del Castillo, T., Ramos, J.L., Rodríguez-Herva, J.J., Fuhrer, T., Sauer, U., Duque, E., 2007. Convergent peripheral pathways catalyze initial glucose catabolism in Pseudomonas putida: genomic and flux analysis. J. Bacteriol. 189, 5142–5152. https://doi.org/10.1128/JB.00203-07.

Dunlop, M.J., Dossani, Z.Y., Szmidt, H.L., Chu, H.C., Lee, T.S., Keasling, J.D., Hadi, M.Z., Mukhopadhyay, A., 2011. Engineering microbial biofuel tolerance and export using efflux pumps. Mol. Syst. Biol. 7, 487. https://doi.org/10.1038/msb.2011.21.

Elmore, J.R., Dexter, G.N., Salvachúa, D., O'Brien, M., Klingeman, D.M., Gorday, K., Michener, J.K., Peterson, D.J., Beckham, G.T., Guss, A.M., 2020. Engineered Pseudomonas putida simultaneously catabolizes five major components of corn stover lignocellulose: glucose, xylose, arabinose, p-coumaric acid, and acetic acid. Metab. Eng. 62, 62–71. https://doi.org/10.1016/j.ymben.2020.08.001.

Eng, T., Herbert, R.A., Martinez, U., Wang, B., Chen, J.C., Brown, J.B., Deutschbauer, A. M., Bissell, M.J., Mortimer, J.C., Mukhopadhyay, A., 2020. Iron supplementation eliminates antagonistic interactions between root-associated bacteria. Front. Microbiol. 11, 1742. https://doi.org/10.3389/fmicb.2020.01742.

Fernández, M., Conde, S., de la Torre, J., Molina-Santiago, C., Ramos, J.-L., Duque, E., 2012. Mechanisms of resistance to chloramphenicol in Pseudomonas putida KT2440. Antimicrob. Agents Chemother. 56, 1001–1009. https://doi.org/10.1128/AAC.05398-11.

Follonier, S., 2015. Pilot-scale production of functionalized mcl-PHA from grape pomace supplemented with fatty acids. Chem. Biochem. Eng. Q. 29, 113–121. https://doi.org/10.15255/CABEQ.2014.2251.

Francis, V.I., Stevenson, E.C., Porter, S.L., 2017. Two-component systems required for virulence in Pseudomonas aeruginosa. FEMS Microbiol. Lett. 364 https://doi.org/10.1093/femsle/fnx104.

Gellatly, S.L., Bains, M., Breidenstein, E.B.M., Strehmel, J., Reffuveille, F., Taylor, P.K., Yeung, A.T.Y., Overhage, J., Hancock, R.E.W., 2018. Novel roles for two-component regulatory systems in cytotoxicity and virulence-related properties in Pseudomonas aeruginosa. AIMS Microbiol 4, 173–191. https://doi.org/10.3934/microbiol.2018.1.173.

Ghiffary, M.R., Prabowo, C.P.S., Sharma, K., Yan, Y., Lee, S.Y., Kim, H.U., 2021. High-level production of the natural blue pigment indigoidine from metabolically engineered corynebacterium glutamicum for sustainable fabric dyes. ACS Sustain. Chem. Eng. https://doi.org/10.1021/acssuschemeng.0c09341.

González-Cabaleiro, R., Mitchell, A.M., Smith, W., Wipat, A., Ofiţeru, I.D., 2017. Heterogeneity in pure microbial systems: experimental measurements and modeling. Front. Microbiol. 8, 1813. https://doi.org/10.3389/fmicb.2017.01813.

Heirendt, L., Arreckx, S., Pfau, T., Mendoza, S.N., Richelle, A., Heinken, A., Haraldsdóttir, H.S., Wachowiak, J., Keating, S.M., Vlasov, V., Magnusdóttir, S., Ng, C.Y., Preciat, G., Žagare, A., Chan, S.H.J., Aurich, M.K., Clancy, C.M., Modamio, J., Sauls, J.T., Noronha, A., Fleming, R.M.T., 2019. Creation and analysis of biochemical constraint-based models using the COBRA Toolbox v.3.0. Nat. Protoc. 14, 639–702. https://doi.org/10.1038/s41596-018-0098-2.

Huang, H., Shao, X., Xie, Y., Wang, T., Zhang, Y., Wang, X., Deng, X., 2019. An integrated genomic regulatory network of virulence-related transcriptional factors in Pseudomonas aeruginosa. Nat. Commun. 10, 2931. https://doi.org/10.1038/s41467-019-10778-w.

Hutchison, C.A., Merryman, C., Sun, L., Assad-Garcia, N., Richter, R.A., Smith, H.O., Glass, J.I., 2019. Polar effects of transposon insertion into a minimal bacterial genome. J. Bacteriol. 201 https://doi.org/10.1128/JB.00185-19.

Incha, M.R., Thompson, M.G., Blake-Hedges, J.M., Liu, Y., Pearson, A.N., Schmidt, M., Gin, J.W., Petzold, C.J., Deutschbauer, A.M., Keasling, J.D., 2020. Leveraging host metabolism for bisdemethoxycurcumin production in Pseudomonas putida. Metab. Eng. Commun. 10, e00119 https://doi.org/10.1016/j.mec.2019.e00119.

Isalan, M., Lemerle, C., Michalodimitrakis, K., Horn, C., Beltrao, P., Raineri, E., Garriga-Canut, M., Serrano, L., 2008. Evolvability and hierarchy in rewired bacterial gene networks. Nature 452, 840–845. https://doi.org/10.1038/nature06847.

Johnson, C.W., Abraham, P.E., Linger, J.G., Khanna, P., Hettich, R.L., Beckham, G.T., 2017. Eliminating a global regulator of carbon catabolite repression enhances the conversion of aromatic lignin monomers to muconate in Pseudomonas putida KT2440. Metab. Eng. Commun. 5, 19–25. https://doi.org/10.1016/j.meteno.2017.05.002.

Johnson, C.W., Salvachúa, D., Rorrer, N.A., Black, B.A., Vardon, D.R., St John, P.C., Cleveland, N.S., Dominick, G., Elmore, J.R., Grundl, N., Khanna, P., Martinez, C.R., Michener, W.E., Peterson, D.J., Ramirez, K.J., Singh, P., VanderWall, T.A., Wilson, A. N., Yi, X., Biddy, M.J., Beckham, G.T., 2019. Innovative chemicals and materials from bacterial aromatic catabolic pathways. Joule. https://doi.org/10.1016/j.joule.2019.05.011.

Linger, J.G., Vardon, D.R., Guarnieri, M.T., Karp, E.M., Hunsinger, G.B., Franden, M.A., Johnson, C.W., Chupka, G., Strathmann, T.J., Pienkos, P.T., Beckham, G.T., 2014. Lignin valorization through integrated biological funneling and chemical catalysis. Proc. Natl. Acad. Sci. U.S.A. 111, 12013–12018. https://doi.org/10.1073/pnas.1410657111.

Maia, P., Rocha, M., Rocha, I., 2016. In silico constraint-based strain optimization methods: the quest for optimal cell factories. Microbiol. Mol. Biol. Rev. 80, 45–67. https://doi.org/10.1128/MMBR.00014-15.

Mallik, D., Pal, S., Ghosh, A.S., 2018. Involvement of AmpG in mediating a dynamic relationship between serine beta-lactamase induction and biofilm-forming ability of Escherichia coli. FEMS Microbiol. Lett. 365 https://doi.org/10.1093/femsle/fny065.

Martínez-Bueno, M.A., Tobes, R., Rey, M., Ramos, J.-L., 2002. Detection of multiple extracytoplasmic function (ECF) sigma factors in the genome of Pseudomonas putida KT2440 and their counterparts in Pseudomonas aeruginosa PA01. Environ. Microbiol. 4, 842–855. https://doi.org/10.1046/j.1462-2920.2002.00371.x.

Mohamed, E.T., Werner, A.Z., Salvachúa, D., Singer, C.A., Szostkiewicz, K., Rafael Jiménez-Díaz, M., Eng, T., Radi, M.S., Simmons, B.A., Mukhopadhyay, A., Herrgård, M.J., Singer, S.W., Beckham, G.T., Feist, A.M., 2020. Adaptive laboratory evolution of Pseudomonas putida KT2440 improves p-coumaric and ferulic acid catabolism and tolerance. Metab. Eng. Commun. 11, e00143 https://doi.org/10.1016/j.mec.2020.e00143.

Molina-Henares, M.A., de la Torre, J., García-Salamanca, A., Molina-Henares, A.J., Herrera, M.C., Ramos, J.L., Duque, E., 2010. Identification of conditionally essential genes for growth of Pseudomonas putida KT2440 on minimal medium through the screening of a genome-wide mutant library. Environ. Microbiol. 12, 1468–1485. https://doi.org/10.1111/j.1462-2920.2010.02166.x.

Mozejko-Ciesielska, J., Pokoj, T., Ciesielski, S., 2018. Transcriptome remodeling of Pseudomonas putida KT2440 during mcl-PHAs synthesis: effect of different carbon sources and response to nitrogen stress. J. Ind. Microbiol. Biotechnol. 45, 433–446. https://doi.org/10.1007/s10295-018-2042-4.

Mutalik, V.K., Novichkov, P.S., Price, M.N., Owens, T.K., Callaghan, M., Carim, S., Deutschbauer, A.M., Arkin, A.P., 2019. Dual-barcoded shotgun expression library sequencing for high-throughput characterization of functional traits in bacteria. Nat. Commun. 10, 308. https://doi.org/10.1038/s41467-018-08177-8.

Nikel, P.I., de Lorenzo, V., 2013. Engineering an anaerobic metabolic regime in Pseudomonas putida KT2440 for the anoxic biodegradation of 1,3-dichloroprop-1-ene. Metab. Eng. 15, 98–112. https://doi.org/10.1016/j.ymben.2012.09.006.

Nogales, J., Mueller, J., Gudmundsson, S., Canalejo, F.J., Duque, E., Monk, J., Feist, A. M., Ramos, J.L., Niu, W., Palsson, B.O., 2020. High-quality genome-scale metabolic modelling of Pseudomonas putida highlights its broad metabolic capabilities. Environ. Microbiol. 22, 255–269. https://doi.org/10.1111/1462-2920.14843.

Norsigian, C.J., Fang, X., Palsson, B.O., Monk, J.M., 2020. Pangenome flux balance analysis toward panphenomes. In: Tettelin, H., Medini, D. (Eds.), The Pangenome: Diversity, Dynamics and Evolution of Genomes. Springer, Cham (CH). https://doi.org/10.1007/978-3-030-38281-0_10.

Pang, B., Chen, Y., Gan, F., Yan, C., Jin, L., Gin, J.W., Petzold, C.J., Keasling, J.D., 2020. Investigation of indigoidine synthetase reveals a conserved active-site base residue of nonribosomal peptide synthetase oxidases. J. Am. Chem. Soc. 142, 10931–10935. https://doi.org/10.1021/jacs.0c04328.

Park, M., Chen, Y., Thompson, M., Benites, V.T., Fong, B., Petzold, C.J., Baidoo, E.E.K., Gladden, J.M., Adams, P.D., Keasling, J.D., Simmons, B.A., Singer, S.W., 2020. Response of Pseudomonas putida to complex, aromatic-rich fractions from biomass. ChemSusChem 13, 1–14. https://doi.org/10.1002/cssc.202000268.

Price, M.N., Ray, J., Iavarone, A.T., Carlson, H.K., Ryan, E.M., Malmstrom, R.R., Arkin, A.P., Deutschbauer, A.M., 2019. Oxidative pathways of deoxyribose and deoxyribonate catabolism. mSystems 4. https://doi.org/10.1128/mSystems.00297-18.

Price, M.N., Wetmore, K.M., Waters, R.J., Callaghan, M., Ray, J., Liu, H., Kuehl, J.V., Melnyk, R.A., Lamson, J.S., Suh, Y., Carlson, H.K., Esquivel, Z., Sadeeshkumar, H., Chakraborty, R., Zane, G.M., Rubin, B.E., Wall, J.D., Visel, A., Bristow, J., Blow, M. J., Deutschbauer, A.M., 2018. Mutant phenotypes for thousands of bacterial genes of unknown function. Nature 557, 503–509. https://doi.org/10.1038/s41586-018-0124-0.

Ravi, K., García-Hidalgo, J., Gorwa-Grauslund, M.F., Lidén, G., 2017. Conversion of lignin model compounds by Pseudomonas putida KT2440 and isolates from compost. Appl. Microbiol. Biotechnol. 101, 5059–5070. https://doi.org/10.1007/s00253-017-8211-y.

Reva, O.N., Weinel, C., Weinel, M., Böhm, K., Stjepandic, D., Hoheisel, J.D., Tümmler, B., 2006. Functional genomics of stress response in Pseudomonas putida KT2440. J. Bacteriol. 188, 4079–4092. https://doi.org/10.1128/JB.00101-06.

Rühl, J., Hein, E.-M., Hayen, H., Schmid, A., Blank, L.M., 2012. The glycerophospholipid inventory of Pseudomonas putida is conserved between strains and enables growth condition-related alterations. Microb. Biotechnol. 5, 45–58. https://doi.org/10.1111/j.1751-7915.2011.00286.x.

Sambrook, J., Russell, D.W., 2001. In: Molecular Cloning: A Laboratory Manual, third ed. Cold Spring Harbor Laboratory Press, Cold Spring Harbor, New York.

Segrè, D., Vitkup, D., Church, G.M., 2002. Analysis of optimality in natural and perturbed metabolic networks. Proc. Natl. Acad. Sci. U.S.A. 99, 15112–15117. https://doi.org/10.1073/pnas.232349399.

Sun, Z., Fridrich, B., de Santi, A., Elangovan, S., Barta, K., 2018. Bright side of lignin depolymerization: toward new platform chemicals. Chem. Rev. 118, 614–678. https://doi.org/10.1021/acs.chemrev.7b00588.

Szklarczyk, D., Gable, A.L., Lyon, D., Junge, A., Wyder, S., Huerta-Cepas, J., Simonovic, M., Doncheva, N.T., Morris, J.H., Bork, P., Jensen, L.J., Mering, C. von, 2019. STRING v11: protein-protein association networks with increased coverage, supporting functional discovery in genome-wide experimental datasets. Nucleic Acids Res. 47, D607–D613. https://doi.org/10.1093/nar/gky1131.

Takahashi, H., Kumagai, T., Kitani, K., Mori, M., Matoba, Y., Sugiyama, M., 2007. Cloning and characterization of a Streptomyces single module type non-ribosomal peptide synthetase catalyzing a blue pigment synthesis. J. Biol. Chem. 282, 9073–9081. https://doi.org/10.1074/jbc.M611319200.

Thompson, M.G., Blake-Hedges, J.M., Cruz-Morales, P., Barajas, J.F., Curran, S.C., Eiben, C.B., Harris, N.C., Benites, V.T., Gin, J.W., Sharpless, W.A., Twigg, F.F., Skyrud, W., Krishna, R.N., Pereira, J.H., Baidoo, E.E.K., Petzold, C.J., Adams, P.D., Arkin, A.P., Deutschbauer, A.M., Keasling, J.D., 2019. Massively parallel fitness profiling reveals multiple novel enzymes in Pseudomonas putida lysine metabolism. mBio 10. https://doi.org/10.1128/mBio.02577-18.

Vercellone-Smith, P., Herson, D.S., 1997. Toluene elicits a carbon starvation response in Pseudomonas putida mt-2 containing the TOL plasmid pWW0. Appl. Environ. Microbiol. 63, 1925–1932. https://doi.org/10.1128/AEM.63.5.1925-1932.1997.

Waskom, M., Gelbart, M., Botvinnik, O., Ostblom, J., Hobson, P., Lukauskas, S., Gemperline, D.C., Augspurger, T., Halchenko, Y., Warmenhoven, J., Cole, J.B., Ruiter, J.D., Vanderplas, J., Hoyer, S., Pye, C., Miles, A., Swain, C., Meyer, K., Martin, M., Bachant, P., Brunner, T., 2020. Mwaskom/Seaborn: v0.11.1 (December 2020). Zenodo. https://doi.org/10.5281/zenodo.4379347.

Wehrs, M., Prahl, J.-P., Moon, J., Li, Y., Tanjore, D., Keasling, J.D., Pray, T., Mukhopadhyay, A., 2018. Production efficiency of the bacterial non-ribosomal peptide indigoidine relies on the respiratory metabolic state in S. cerevisiae. Microb. Cell Factories 17, 193. https://doi.org/10.1186/s12934-018-1045-1.

Wehrs, M., Tanjore, D., Eng, T., Lievense, J., Pray, T.R., Mukhopadhyay, A., 2019. Engineering robust production microbes for large-scale cultivation. Trends Microbiol. 27, 524–537. https://doi.org/10.1016/j.tim.2019.01.006.

Wehrs, M., Thompson, M.G., Banerjee, D., Prahl, J.-P., Morella, N.M., Barcelos, C.A., Moon, J., Costello, Z., Keasling, J.D., Shih, P.M., Tanjore, D., Mukhopadhyay, A., 2020. Investigation of Bar-seq as a method to study population dynamics of Saccharomyces cerevisiae deletion library during bioreactor cultivation. Microb. Cell Factories 19, 167. https://doi.org/10.1186/s12934-020-01423-z.

Wetmore, K.M., Price, M.N., Waters, R.J., Lamson, J.S., He, J., Hoover, C.A., Blow, M.J., Bristow, J., Butland, G., Arkin, A.P., Deutschbauer, A., 2015. Rapid quantification of mutant fitness in diverse bacteria by sequencing randomly bar-coded transposons. mBio 6, e00306–e00315. https://doi.org/10.1128/mBio.00306-15.

Whistler, C.A., Corbell, N.A., Sarniguet, A., Ream, W., Loper, J.E., 1998. The two-component regulators GacS and GacA influence accumulation of the stationary-phase sigma factor sigmaS and the stress response in Pseudomonas fluorescens Pf-5. J. Bacteriol. 180, 6635–6641. https://doi.org/10.1128/JB.180.24.6635-6641.1998.

Zhu, L., Li, Y., Wang, J., Wang, X., 2017. Identification of two secondary acyltransferases of lipid A in Pseudomonas putida KT2442. J. Appl. Microbiol. 123, 478–490. https://doi.org/10.1111/jam.13499.